Chapter 3

Preparation and Reactivity of Mesoionic Carbene (MIC)–Containing Ruthenium Metathesis Catalysts and their Acid-Activated Behavior

The text in this chapter is reproduced in part with permission from:

Bouffard, J.; Keitz, B. K.; Tonner, R.; Guisado-Barrios, G.; Frenking, G.; Grubbs, R. H.; Bertrand, G. *Organometallics* **2011**, *30*, 2617.

Keitz, B. K.; Bouffard, J.; Bertrand, G.; Grubbs, R. H. *J. Am. Chem. Soc.* **2011**, *133*, 8498.

Abstract

The preparation of mesoionic carbenes (MICs) from the cycloaddition of 1,3-diaza-2-azoniaallenes and alkynes is described, as is their use as ligands in ruthenium olefin metathesis catalysts. These MIC-ligated catalysts displayed reactivities in ring-opening metathesis polymerization (ROMP) and ring-closing metathesis (RCM) comparable to that of their N-heterocyclic carbene (NHC)-based counterparts.

Specific MICs exhibited unique protonolysis behavior, which resulted in dissociation of the MIC from the ruthenium center. Taking advantage of this phenomenon, we describe the development of extremely stable and reactive acid-activated metathesis catalysts. Detailed mechanistic studies on the activation mechanism and reactivity comparisons to previously reported metathesis catalysts are also presented.

MIC-Based Ruthenium Olefin Metathesis Catalysts

Introduction

Like many organometallic complexes, the activity and stability of ruthenium metathesis catalysts depends on the nature of the ligands connected to the metal.[1] For instance, the identity of the dissociating ligand, whether a phosphine (**3.2**) or oxygen (**3.3**) has a significant effect on catalyst stability by enabling or disabling specific decomposition pathways.[2] Similarly, the ligand that remains attached to the metal throughout the catalytic cycle has a significant effect on catalyst initiation, propagation, and selectivity (Chapters 4 and 5).[3] As a specific

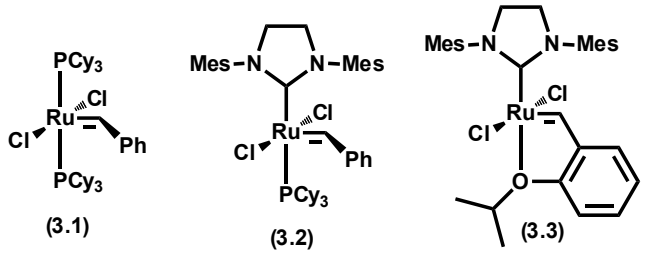

Figure 3.1. Common ruthenium olefin metathesis catalysts. Mes = 2,4,6-trimethylbenzene

example, consider the reactivity differences between catalysts **3.1** and **3.2**. The phosphine-containing catalyst **3.1** initiates much faster (large k of phosphine dissociation) than the NHC-based catalyst **3.2** (small k of phosphine dissociation), yet **3.2** is considerably more active. The explanation is that **3.2** has a much higher preference for olefin binding compared to **3.1**, and thus appears to react faster. From this result, as well as those presented in the following chapters of this thesis, it is clear that the L-type ligand has a significant effect on catalyst activity. Thus, despite the difficulties in quantitatively relating the properties of this ligand to catalyst properties,[4] it has become a favored target for catalyst optimization.[5]

Among NHC-type ligands (Figure 3.2), many sub-types have been explored in the context of metathesis chemistry, including saturated/unsaturated (**3.4**),[6] abnormal (aNHCs, **3.6**),[7] and cyclic alkyl amino carbenes (CAACs, **3.5**).[8] Abnormal NHCs, where the carbene center is not adjacent to a donor atom (e.g., nitrogen), are part of a larger subclass of NHCs termed mesoionic carbenes (MICs, **3.6** and **3.7**). Their name is derived from the fact that a canonical resonance form of the carbene cannot be drawn without the introduction of formal charges.[9] While MICs based on imidazolium salts (two nitrogen atoms in the ring) and their metal complexes are well known,[10] triazolium-derived MICs (containing three nitrogen

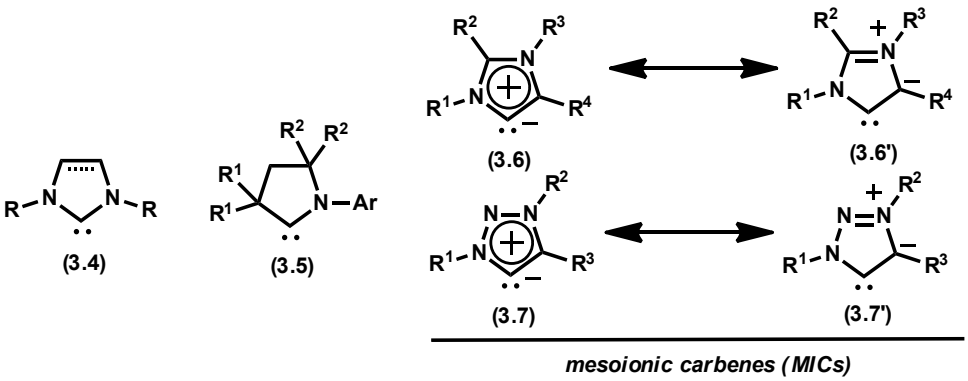

Figure 3.2. Various stable carbene species including traditional N-heterocylic carbenes (NHCs, **3.4**), cyclic-alkyl amino carbenes (CAACs, **3.5**), and mesoionic carbenes (MICs, **3.6** and **3.7**)

atoms in the ring) are less common, despite their availability from Cu-catalyzed azide-alkyne cycloaddition ('click') chemistry. However, the Bertrand group has recently reported the facile preparation of stable, triazolium-derived MICs and their incorporation into simple metal complexes.[11] The distinct electronic properties of these carbenes, mainly their greater σ-donation and decreased π-accepting ability (compared to **3.6**), along with their reduced susceptibility to decomposition via dimer formation made them attractive targets for incorporation into metathesis catalysts.[12] Thus, in this chapter, we describe the preparation and activity of ruthenium metathesis catalysts containing stable MICs. We also demonstrate that certain MICs undergo facile protonolysis when attached to the ruthenium center, and that this ability can be used as the basis for an acid-activated metathesis catalyst.

Results and Discussion

As previously mentioned, triazolium salt precursors to carbenes like **3.7** can

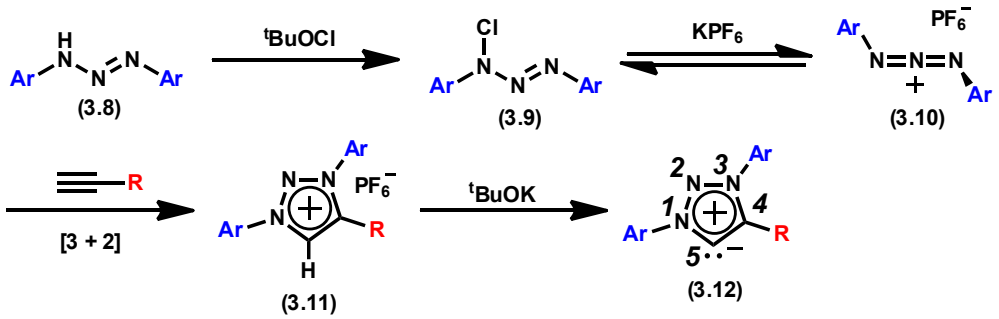

Figure 3.3. Preparation of 1,3-diaryl-1,2,3-triazolium salts (**3.11**) via the [3+2] cycloaddition of triazenes (**3.10**) with terminal alkynes and their deprotonation to give stable MICs (**3.12**)

be readily prepared by click chemistry followed by alkylation at the N3 position. Unfortunately, the 1,3-*dialkyl*-1,2,3-triazolium salts that are most amenable to this chemistry do not give stable MICs upon deprotonation. As a result, they are challenging to incorporate into organometallic complexes. In contrast, the Bertrand group has recently reported that *diaryl* triazolium salts yield stable and isolable MICs upon deprotonation at low temperature with potassium *tert*-butoxide (KO^{t}Bu).[11] While these salts cannot be prepared through traditional Click chemistry, they are readily synthetized from the cycloaddition of chloro-triazenes and alkyne or alkyne equivalents (vinyl halides) (Figure 3.3). Using this methodology, a wide variety of differentially substituted MICs were prepared and fully characterized by ^{1}H and ^{13}C NMR spectroscopy. Their electronic structure was also studied using density functional theory (DFT).[13] Thus, having established the synthesis and electronic structure of several MICs, we turned our attention to their application as ligands in ruthenium olefin metathesis catalysts.

Free MICs of the type **3.12** bearing flanking aryl groups of varying steric demand were selected for the synthesis of new metathesis catalysts via simple

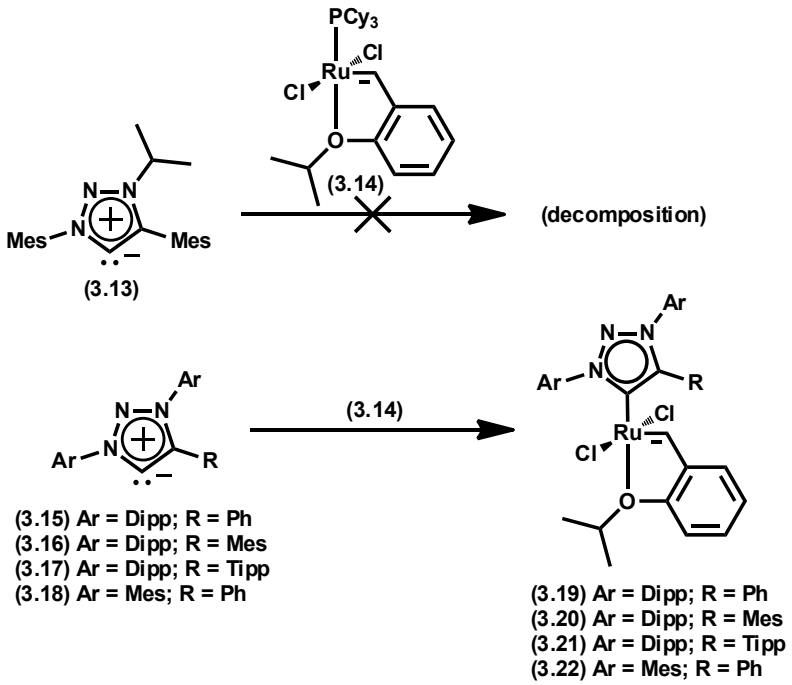

Figure 3.4. Synthesis of ruthenium complexes (**3.19**-**3.22**) via ligand substitution with MICs (**3.15**-**3.18**). Dipp = 2,6-diisopropylphenyl, Tipp = 2,4,6-triisopropylphenyl

ligand substitution of **3.14**. The new complexes represent MIC-based analogues of the standard NHC-based metathesis catalysts (e.g., **3.3**). Early attempts using the MIC **3.13** alkylated at N3 resulted in complete decomposition of **3.14** as evidenced by the disappearance of the benzylidene ^{1}H resonance. Gratifyingly, the use of more robust MICs arylated at N3 (**3.15**–**3.18**) provided the desired catalysts (**3.19**–**3.22**). For example, combining a free MIC with complex **3.14** in benzene resulted in complete consumption of the starting ruthenium catalyst within a few hours. The resulting catalysts were isolated by recrystallization from CH_2Cl_2-pentane (**3.19**, **3.20**, **3.22**) or pentane (**3.21**) at –30 °C without the need for column chromatography. Complexes **3.19**–**3.22** were found to decompose relatively quickly in solution (within 6 h) upon exposure to oxygen, but were indefinitely

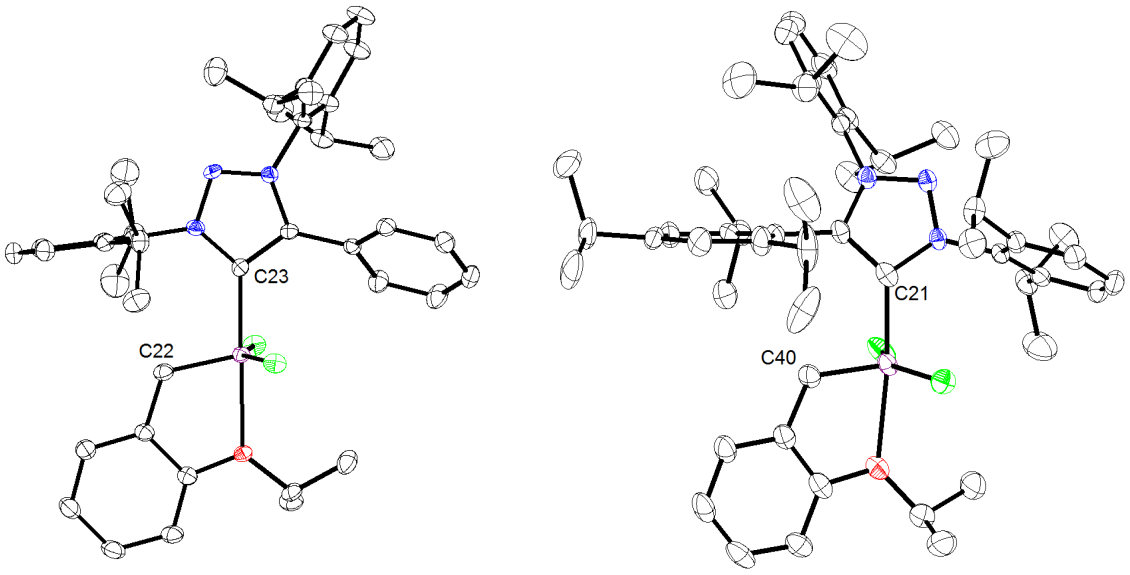

Figure 3.5. Solid-state structures of **3.19** (left) and **3.21** (right) with 50% thermal ellipsoids. Selected bond lengths (Å) for **3.19**: C23-Ru: 1.9913(1), C22-Ru: 1.8235(1), O-Ru: 2.2696(1). For **3.21**: C21-Ru: 1.9852(1), C40-Ru: 1.8157(1), O-Ru: 2.3176(1)

stable in the solid state under an inert atmosphere. NMR spectroscopy studies on the ligand displacement reaction with **3.14** indicated that a MIC-phosphine complex where the MIC initially displaces the chelating ether moiety in **3.14** was formed before subsequently yielding the desired complex.[14] This intermediate usually persisted for several hours before forming the desired complex (*vide infra*).

Complexes **3.19** and **3.21** were characterized by single-crystal x-ray diffraction (Figure 3.5) after crystallizing from slow evaporation of a saturated CH_2Cl_2 solution. The bond lengths in **3.19** and **3.21** are very similar to those found in **3.3**. For example, the MIC carbon – Ru bond length (1.99 Å versus 1.98 Å in **3.3**), the benzylidene C – Ru bond length (1.82 Å versus 1.82 Å) and the O – Ru bond length (2.27 Å versus 2.26 Å) are largely conserved across the three species.[15] Notably, the smaller aryl substituent (on C4 in **3.19** and N1 in **3.21**) is positioned above the

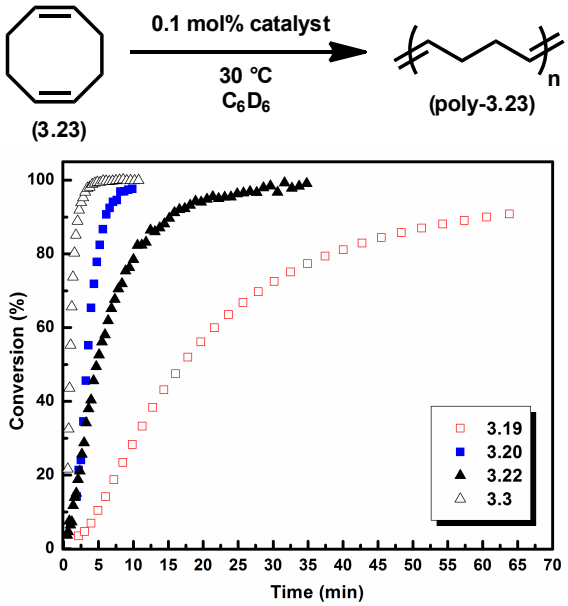

Figure 3.6. ROMP of cyclooctadiene (**3.23**) with MIC-catalysts **3.19**, **3.20**, and **3.22**

Table 3.1. Comparison of activation parameters for catalysts **3.19**–**3.22**[a]

Catalyst	$\Delta G^{\ddagger}$, kcal·mol^{-1}	$\Delta H^{\ddagger}$, kcal·mol^{-1}	$\Delta S^{\ddagger}$, eu
3.19	21.6 ± 0.8	12.1 ± 0.5	–31.9 ± 1.5
3.20	20.2 ± 0.2	13.5 ± 0.8	–22.5 ± 2.7
3.21	23.5 ± 0.1	13.6 ± 0.6	–33.0 ± 1.9
3.22	20.8 ± 0.3	14.6 ± 0.5	–21 ± 1.6

[a] Conditions: catalyst (0.003 mmol), butyl vinyl ether (0.09 mmol, 0.15 M) in d_8-toluene at varying temperatures

Cl-Ru-Cl plane in order to minimize steric interactions with the chlorines, while the large substituent is positioned above the benzylidene.[16] Thus, in the solid state, **3.19** and **3.21** exist as distinct rotamers. For the most part, the crystal structures of the MIC catalysts were unremarkable and did not provide any insight into their reactivity.

To evaluate the catalytic activity of the MIC-catalysts, they were subjected to several standard metathesis screens.[17] Catalysts **3.19**, **3.20**, and **3.22** showed good ring-opening metathesis polymerization (ROMP) activity (Figure 3.6), while

catalyst **3.21** reached only low conversions, even after a period of several days. Comparing the ROMP conversion profiles of MIC-based catalysts to standard catalyst **3.3** revealed a few similarities and differences. For instance, **3.20** displayed a very similar conversion profile to **3.3**, while **3.22** is slightly slower, but still relatively fast, and **3.19** is much slower, although it does reach 100% conversion after ca. 1 h.

The most surprising result is the difference in reactivity between catalysts **3.19** and **3.20**, since the only distinction between the two is the substitution of a Mes group for a phenyl at C4. We hypothesized that the observed behavior might be largely due to a difference in initiation rates, and in order to probe this, we constructed several Eyring plots for the reaction of each catalyst with butyl vinyl ether.[2,18] The results of the initiation parameters are given in Table 3.1. Catalysts **3.19**–**3.22** all exhibited a negative entropy of activation ($\Delta S^{\ddagger}$), which is consistent with an associative or associative interchange mechanism previously reported for catalysts incorporating a Hoveyda-type chelate (e.g., **3.3**).[19]

Interestingly, while **3.19** and **3.21** were found to have very similar activation entropies, catalysts **3.20** and **3.22** different by ca. 10 entropy units (eu) from these. Furthermore, the activation enthalpy ($\Delta H^{\ddagger}$) for **3.19** was found to be lower than that of **3.20**. Nevertheless, a 1.4 kcal·mol^{-1} difference in the free energy of activation ($\Delta G^{\ddagger}$) between **3.19** and **3.20** was observed when combining the $\Delta H^{\ddagger}$ and $\Delta S^{\ddagger}$ parameters at RT. This difference accounts nicely for the observed variations in initiation while also explaining the almost complete inactivity of catalyst **3.21** at RT. Unfortunately, while it is clear that sterics play a significant role in catalyst initiation and activity, so far a quantitative structural model that accounts for the observed

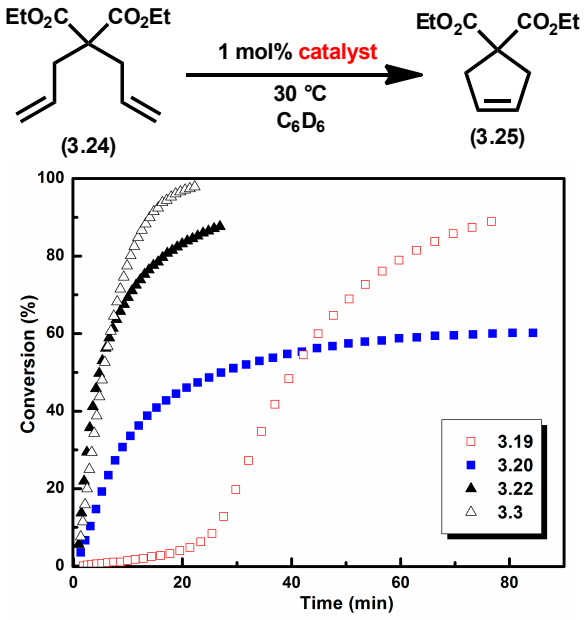

Figure 3.7. RCM performance of catalysts **3.19**, **3.20**, **3.22**, and **3.3**

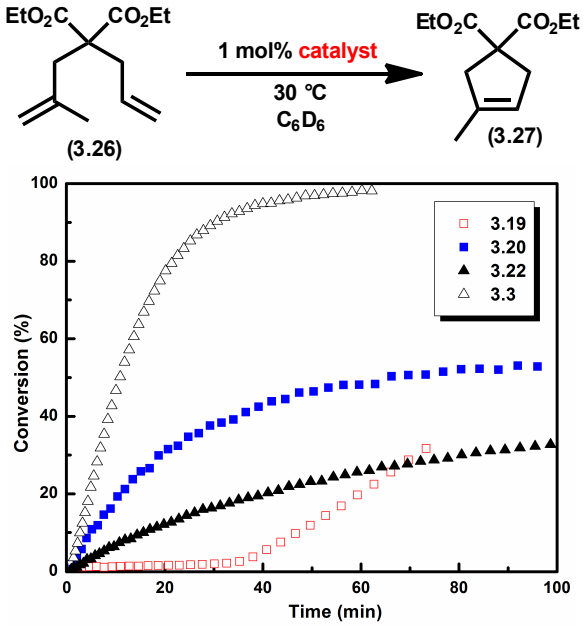

Figure 3.8. Trisubstituted RCM performance of catalysts **3.19**, **3.20**, **3.22**, and **3.3**

differences in initiation, particularly between **3.19** and **3.20**, has eluded us.[13]

Following our initiation rate studies, the performance of each catalyst in ring-closing metathesis (RCM) was assessed. Again, catalyst **3.21** was

found to be almost completely inactive at 30 °C. The other catalysts displayed conversion profiles consistent with their initiation activation energies. For instance, **3.20** shows a fast increase in conversion followed by a plateau that most likely results from catalyst decomposition. On the other hand, catalyst **3.19** exhibits an induction period characteristic of slow initiation followed by a gradual increase toward 100% conversion. Notably, even though **3.19** initiates at a slower rate than **3.20**, it is able to reach 100% conversion under the examined conditions while **3.20** is not. The best performing MIC-catalyst in the RCM assay was **3.22**, which displayed fast initiation and good stability throughout the reaction. In fact, **3.22** closely matched the performance of **3.3**.

To further examine the differences in reactivity between the catalysts, trisubstituted RCM was attempted (Figure 3.8). As expected, **3.19** and **3.20** exhibited the same relative behavior as stated above, with **3.19** displaying a lengthy induction period, while **3.20** began conversion to product almost immediately. Catalyst **3.20** reached a maximum conversion of ca. 50% while **3.19** was able to reach 100% conversion after a period of ca. 16 h. These results confirm that not only does the change from Ph (**3.19**) to Mes (**3.20**) have a profound effect on the initiation rate but it also impacts the relative stability of the catalysts. Catalyst **3.22** was relatively sluggish over the time period examined but was able to reach 100% after ca. 24 h at 30 °C. Overall, in the trisubstituted RCM assay, the MIC-based catalysts were clearly inferior to **3.3**, in contrast to the previous assays, where they displayed similar activity.

Conclusion and Future Outlook

The enhanced stability of N-arylated MICs allowed for the preparation of new ruthenium olefin metathesis catalysts via simple ligand substitution. These catalysts were proficient at the ROMP of cyclic olefins and at RCM reactions leading to both di- and trisubstituted cyclic olefins. In general, the catalytic properties of the MIC-Ru complexes, in particular with respect to their rates of initiation and resistance to deactivation, were found to be strongly influenced by the nature of the MIC substituents and in several cases rivaled the performance of well-established NHC-based ruthenium metathesis catalysts. In conclusion, the combination of their practical, versatile, and modular preparation, enhanced stability, and the demonstration of their effectiveness in a catalytic setting foreshadows the development of MIC transition metal complexes for numerous catalytic applications, including olefin metathesis.

Acid-Activated, MIC-Based Ruthenium Metathesis Catalysts

Introduction

The motivation behind the preparation of latent metathesis catalysts was discussed in Chapter 2. In that chapter, several examples of catalysts that relied on protonation and subsequent displacement of a labile ligand in order to generate an active species were presented. Unfortunately, these catalysts were oxygen-sensitive and could only be prepared with toxic metal salts. In order to address these deficiencies, we sought to prepare superior acid-activated catalysts based on a bis-NHC motif. Here, we report that ruthenium complexes incorporating a

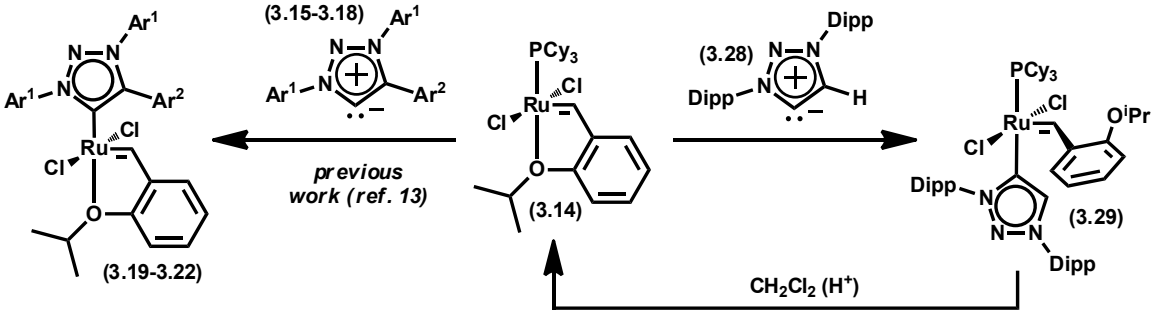

Figure 3.9. Initial discovery of acid-induced dissociation of MIC **3.28** from **3.29** (Dipp = 2,6-diisopropylphenyl)

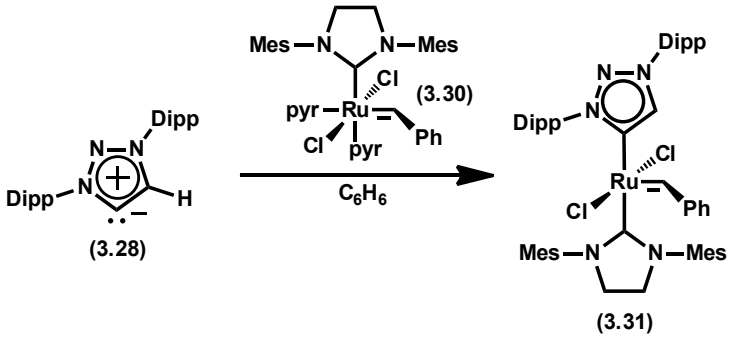

Figure 3.10. Preparation of **3.31** from MIC **3.28** and **3.30**. pyr = pyridine

traditional NHC and a MIC (see above) may be activated by the addition of a Brønsted acid. The resulting catalyst combines the stability and latency of bis-NHC complexes while maintaining low activation temperatures. Furthermore, we demonstrate that in some reactions, the performance of this catalyst surpasses that of the best commercially available catalysts (e.g., **3.3**).

Results and Discussion

Previously in this chapter, we reported the synthesis and activity of ruthenium olefin metathesis catalysts bearing MICs (**3.19**–**3.22**) in place of more traditional NHCs (Figure 3.4). In our attempts to prepare analogues bearing the unhindered H-substituted (at C4) MIC **3.28** from **3.14**, we observed the formation of compound

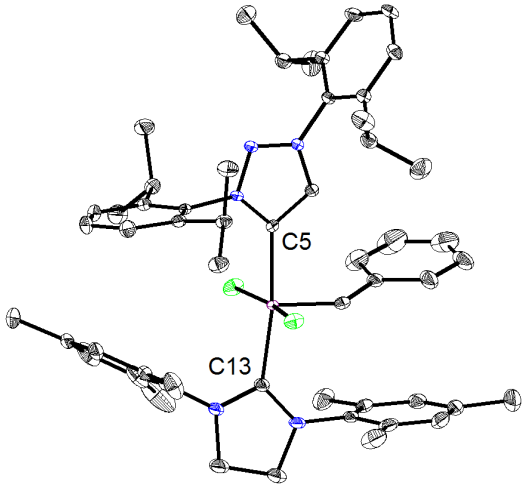

Figure 3.11. Solid-state structure of **3.31** with 50% probability ellipsoids. H atoms have been omitted for clarity. Selected bond lengths (Å) and angle (deg): C13 – Ru, 2.086, C5 – Ru, 2.097, C13 – Ru – C5, 169.34

3.29. In contrast to similar intermediates observed during the metalation of MICs **3.15**–**3.18**, compound **3.29** was indefinitely stable and phosphine dissociation never occurred to give the desired MIC catalyst. However, we noticed that in the presence of a solvent containing acidic impurities, the transformation of **3.29** to **3.14** occurred, a reaction that represents the formal protonolysis of a metal-NHC bond (Figure 3.9). Although relatively rare, protonolysis reactions of metal-NHC bonds have been observed for ruthenium and other late metals.[20,21] Given these precedents, we concluded that MIC **3.28** was acid-labile and imagined that it could be incorporated into a metathesis catalyst as a dissociating ligand.

Combining free MIC **3.28** with **3.30** in C_6H_6 resulted in the new complex **3.31**, which was isolated in excellent yield after washing with cold pentane (Figure 3.10). Crystals of **3.31** suitable for x-ray diffraction were grown from slow diffusion of pentane onto a saturated toluene solution of **3.31**. The solid-state structure of **3.31** (Figure 3.11) was consistent with previously reported bis-NHC complexes

Table 3.2. RCM of **3.24** with **3.31** (1 mol%) and acid (ca. 20 mol%) in C_6D_6 (0.1 M)[a]

entry	acid	time, h	conv., %[a]
1	None	18+	<5
2	HCl (1 M in Et_2O)	0.3	>95
3	Perchloric (70%)	4	73
4	Trifluoroacetic	0.3	>95
5	Acetic	18	20
6	Formic (88%)	18	91
7	Hydrobromic (48%)	4	>95
8	Hydroiodic (57%)	4	>95
9	HBF_4 (Et_2O)	1	16
10	BH_3 (THF)	18	19
11	$B(C_6F_5)_3$	17	33
12	$ZnCl_2$	1	>95
13	$SnCl_4$	18	<5

[a] measured by ^1H NMR spectroscopy

and MIC-Ru complexes (**3.19** and **3.21**).

Initial metathesis screens revealed that **3.31** is completely inactive at RT. For instance, 1 mol% of **3.31** in C_6H_6 was unable to polymerize 1,5-cyclooctadiene (**3.23**) to any detectable extent within a period of 12 h at RT.[22] Some minimal conversion was observed after extended periods, presumably as a result of very slow catalyst initiation due to acidic glassware or acid impurities. Under similar reaction conditions, < 5% conversion of the RCM substrate **3.24** was observed over a period of several weeks at RT. In contrast, addition of HCl (1 M in Et_2O) resulted in complete and immediate conversion of **3.24** to the RCM product **3.25** within 20 min (Table 3.2, entry 2). Having established the feasibility of our initial hypothesis, we set about studying the protonolysis reaction in greater detail.

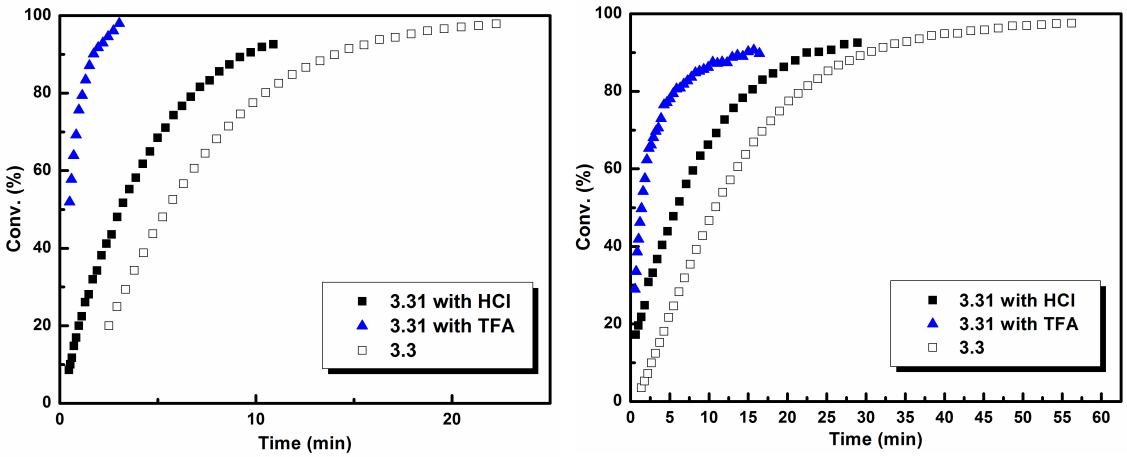

Figure 3.12. (left) RCM of **3.24** with **3.31** and TFA (blue triangles) or HCl (black squares) and RCM of **3.24** with **3.3** (white squares). Conditions: **3.24** (0.08 mmol), **3.31** or **3.3** (0.0008 mmol), and HCl (1 M in Et_2O, 31 equiv., 0.025 mmol) or TFA (160 equiv., 0.130 mmol) in C_6D_6 (0.8 mL) at 30 °C. (right) RCM of **3.26** with **3.31** and TFA (blue triangles) or HCl (black squares) and RCM of **3.26** with **3.3** (white squares). Conditions: **3.26** (0.08 mmol), **3.31** or **3.3** (0.0008 mmol), and HCl (1 M in Et_2O, 31 equiv., 0.025 mmol) or TFA (160 equiv., 0.130 mmol) in C_6D_6 (0.8 mL) at 30 °C. Conversion was measured by ^1H NMR spectroscopy

Table 3.3. Polymerization results with catalyst **3.31**[a]

Solvent	Monomer	Acid	[Monomer], M	[3.31], M	[Acid], M[a]	M_n, g/mol[b]	PDI
PhH	**3.32**	TFA	0.26	0.003	0.04	12,000	1.42
PhH	**3.32**	MSA	0.26	0.003	0.04	19,000	1.53
PhH	**3.32**	HCl	0.5	0.0005	0.059	42,000	1.48
PhH	**3.32**	HCl	0.5	0.0005	0.08	29,500	1.65
PhH	**3.23**	HCl	0.5	0.001	0.059	50,000	1.48
$PhCH_3$	**3.23**	HCl	0.5	0.001	0.059	31,000	1.47

[a] HCl was added as a 1 M solution in Et_2O. MSA = methane sulfonic acid. [b] Molecular weights measured by multi-angle laser light scattering (MALS) GPC

Our initial efforts focused on the effects of different acids on the RCM of **3.24** (Table 3.2). Strong acids (entries 2–4, 7, and 8) were found to be the most effective and were capable of initiating the reaction even when added as aqueous solutions. However, the identity of the conjugate base was also important, as HBF_4

performed poorly (entry 9) in comparison to acids with similar pK_a's. A similar result was observed for the *acac*-based, acid-activated complexes presented in Chapter 2. Weaker acids (entries 5 and 6) were less efficient and reached full conversion only after several hours or not at all. Interestingly, some Lewis acids were also capable of affecting the transformation. For instance, addition of $ZnCl_2$ resulted in complete conversion with 2 h at RT, while addition of $B(C_6F_5)_3$ resulted in only 33% conversion after several hours. Other Lewis acids such as $SnCl_4$ were found to be even less effective. In general, Brønsted acids significantly outperformed Lewis acids.

Because of their proficiency in activating **3.31**, HCl and trifluoroacetic acid (TFA) were chosen to investigate the RCM of **3.24** to **3.25** more closely. Under standard RCM screening conditions, a mixture of **3.31** and either HCl or TFA showed complete conversion of **3.24** to **3.25** within 10 min at 30 °C (Figure 3.12, left). The reaction with TFA was particularly fast, reaching 100% conversion within only a few minutes. Catalyst **3.31** also excelled at the RCM of trisubstituted substrate **3.26** (Figure 3.12, right). Notably, in the above RCM reactions, catalyst **3.31** was found to be superior to commercial catalysts such as (H_2IMes)Cl_2Ru(=CHPhO^{i}Pr) (**3.3**, H_2IMes = 1,3-dimesitylimidazolidin-2-ylidene).[23] As expected on the basis of these results, **3.31** also performed exceptionally well at the ring-opening metathesis polymerization (ROMP) of **3.23** and *cis*-cyclooctene (**3.32**) with both HCl and TFA as activators (Table 3.3). Molecular weights (M_n) were largely consistent with the predicted values and molecular weight distributions (PDI) were comparable to those obtained from the ROMP of **3.23** and **3.32** with

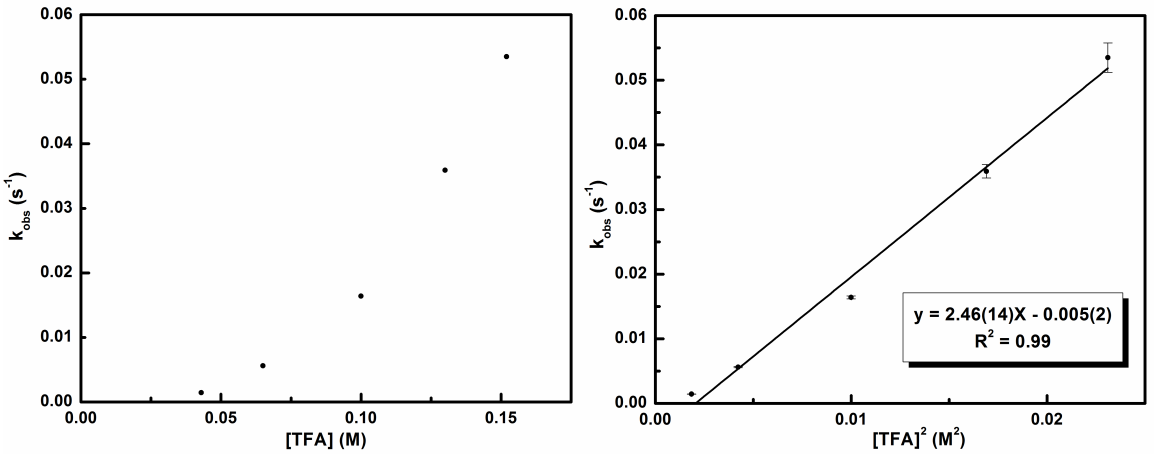

Figure 3.13. Observed rate constant versus [TFA] (left) and $[TFA]^2$ showing 2nd -order dependence on [TFA]

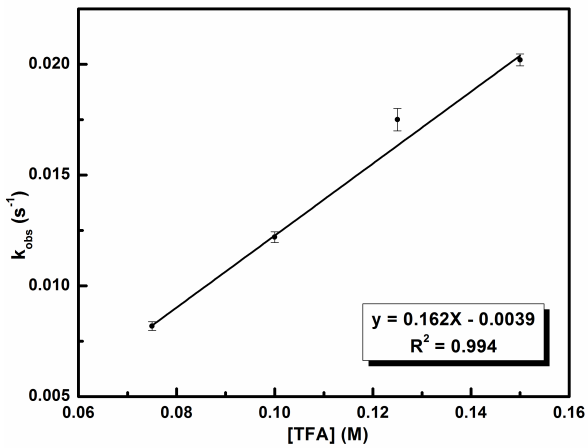

Figure 3.14. Observed rate constant versus [TFA] in CD_3CN at RT and constant pH. Conditions were **3.31** (0.003 mmol), KTFA (0.003–0.006 mmol), and TFA (0.045–0.09 mmol) in CD_3CN (0.6 mL)

catalysts **3.2** and **3.3**.[24]

After the activation of **3.31** had been established, additional experiments were performed with the two best acid activators, TFA and HCl, to study the mechanism of activation in greater detail. The benzylidene proton resonance of **3.31** was monitored by ^1H NMR spectroscopy following the addition of varying amounts of TFA. A plot of the observed rate constant (k_{obs}) versus concentration of TFA in C_6D_6 displayed a second-order dependence on TFA concentration (Figure

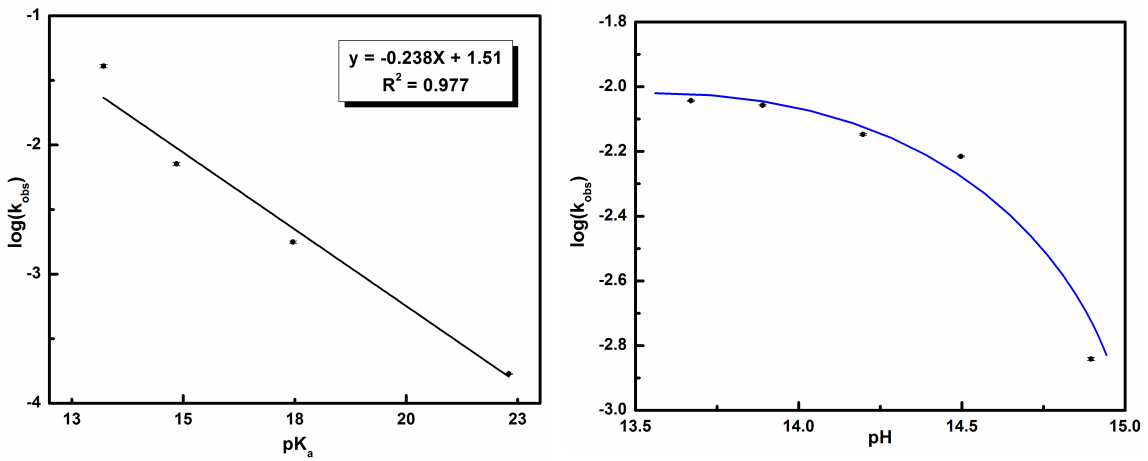

Figure 3.15. (left) Bronsted plot for initiation of **3.31** at RT in CD_3CN. Conditions: **3.31** (0.003 mmol) and acid (0.045 mmol) in CD_3CN (0.6 mL). Acids were acetic acid, Cl_2HCCO_2H, F_3CCO_2H (TFA), and CH_3SO_3H (MSA). (right) log(kobs) versus pH for reaction of **3.31** with TFA in CD3CN. Blue line represents ideal curve based on pK_a of TFA in CD_3CN

3.13). This behavior is consistent with protonation of **3.31** by an acid dimer instead of an acid monomer. Indeed, carboxylic acids are known to form dimers via hydrogen bonding in hydrocarbon solvents such as PhH and $PhCH_3$.[25] However, in order for the above situation to be plausible, protonation must be involved in the rate-determining step of the reaction. To probe this possibility and also to simplify the acid – base chemistry of the system, we decided to monitor the initiation of **3.31** in CD_3CN rather than in C_6D_6.

If protonation is involved in the rate-determining step of the initiation reaction, a plot of k_{obs} versus acid concentration should be linear *at constant pH*.[26] This would parallel the behavior of general acid-catalyzed reactions, although in this case, kinetic runs were conducted under pseudo-first-order conditions. When an initiation study was performed with TFA in CD_3CN using potassium trifluoroacetate (KTFA) to maintain an approximately constant pH, a linear plot was obtained

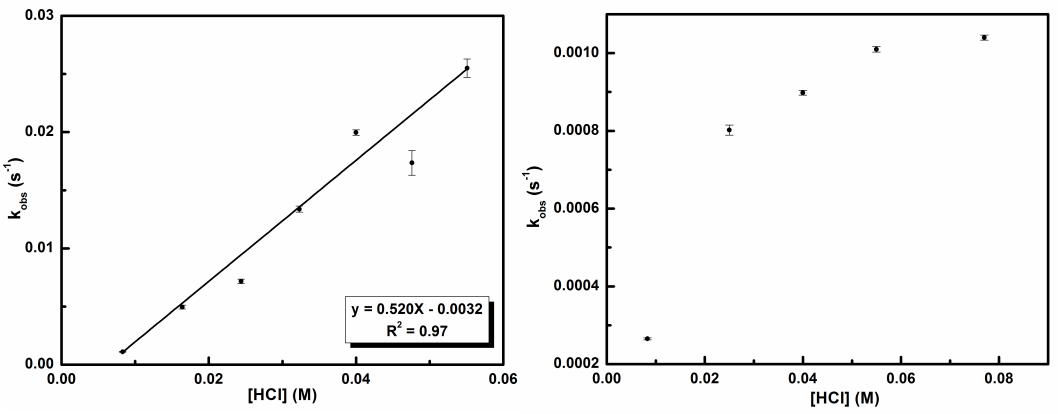

Figure 3.16. (left) Plot of k_{obs} versus [HCl] for reaction of **3.31** with HCl in CD_3CN. (right) Plot of k_{obs} versus [HCl] in C_6D_6. Conditions were **3.31** (0.003 mmol), and C_6D_6 (0.6 mL) with varying amounts of HCl (0.0083 M–0.077 M)

(Figure 3.14). Further evidence of the involvement of acid in the rate-determining step was provided by a Brønsted plot (Figure 3.15, left), which displays a linear relationship between the pK_a of the acid in CD_3CN and the logarithm of the initiation rate of **3.31**.[27] Finally, a plot of log(k_{obs}) versus the pH of the solution exhibited behavior characteristic of the involvement of acid in the rate-determining step (Figure 3.15, right). When HCl was used in place of TFA in CD_3CN, a first-order dependence on HCl concentration was observed (Figure 3.16, left). All of the above results are strong indications that a protonation event rather than dissociation is the rate-determining step in catalyst activation.

Compared to the initiation experiments conducted in CD_3CN, the initiation mechanism of **3.31** in the presence of inorganic acids in solvents of lower polarity (C_6D_6, toluene-d_8) is far more complex and likely involves poorly understood solvation and/or counterion effects, as suggested from the screening of acid initiators (Table 3.2). For instance, the reaction of **3.31** in C_6D_6 following the addition of excess HCl (> 15 equiv) resulted in a decrease in the benzylidene proton signal

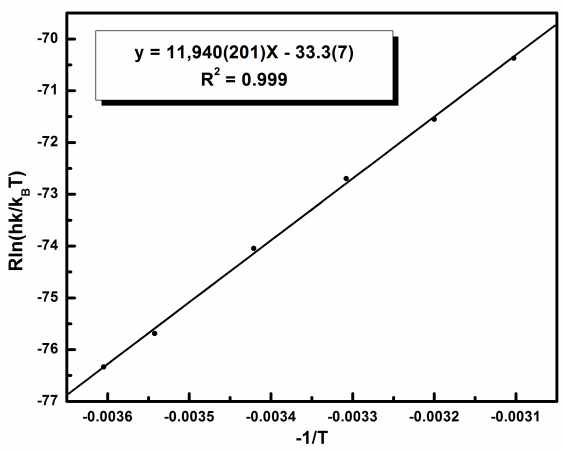

Figure 3.17. Eyring plot for activation of **3.31** at saturation conditions with HCl and toluene-d_8

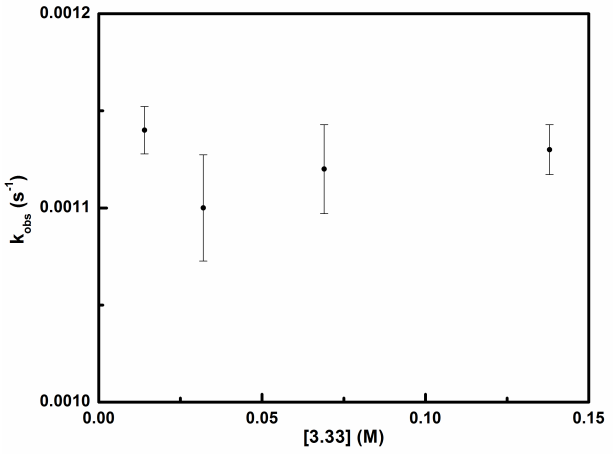

Figure 3.18. Plot of k_{obs} versus [**3.33**] in C_6D_6. Conditions were **3.31** (0.003 mmol) and HCl (1 M in Et_2O, 0.077 m) in C_6D_6 (0.6 mL) with varying amounts of **3.33** (0.014 M–0.14 M)

intensity that followed clean first-order kinetics. A plot of k_{obs} versus HCl concentration displayed saturation kinetics, which is inconsistent with a protonation event being rate-determining under these conditions and *may* be indicative of a pre-equilibrium step (Figure 3.16, right). However, a more likely explanation is that the saturation behavior is due to the limited solubility of HCl in the hydrocarbon solvents under study, since in CD_3CN a linear dependence of k_{obs} on [HCl] was observed.[28] In

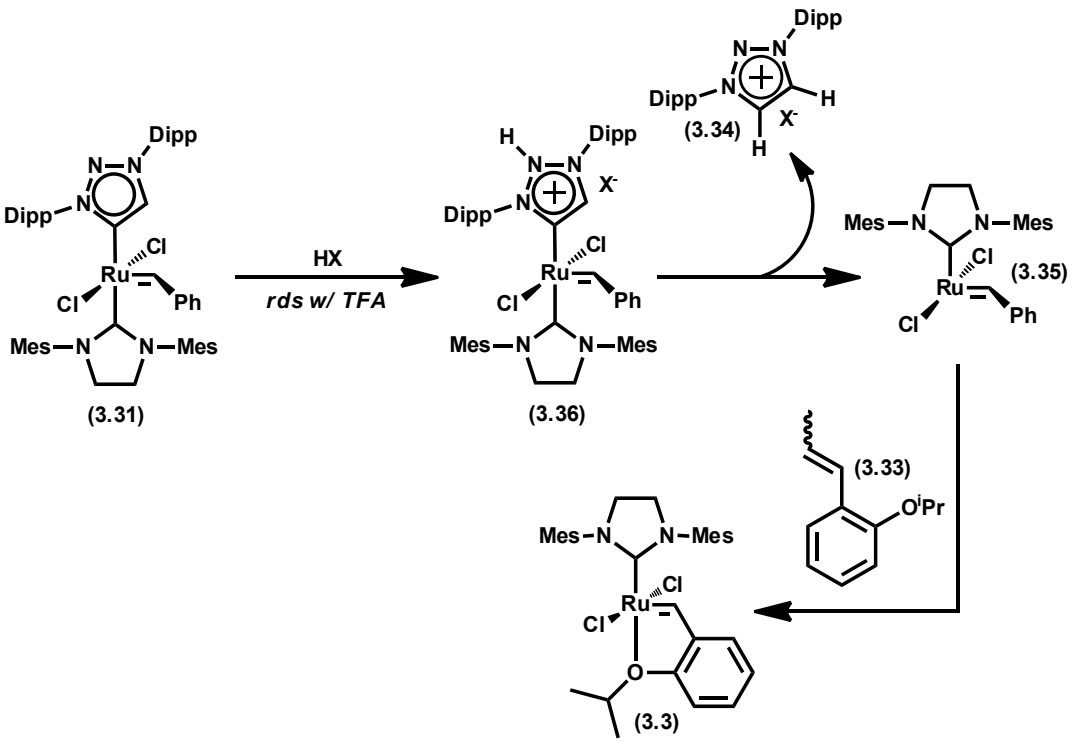

Figure 3.19. Proposed mechanism for initiation of **3.31**

support of this, we note that an Eyring plot of the activation reaction with HCl in toluene-d_8 under saturation conditions (Figure 3.17) yielded the values $\Delta H^{\ddagger}$ = 11.9 ± 0.2 kcal/mol and $\Delta S^{\ddagger}$ = -33.3 ± 0.7 eu, which are inconsistent with the description of the above saturation kinetics as a fast protonation equilibrium followed by a slow ligand dissociation. However, any conclusions based on $\Delta S^{\ddagger}$ alone are complicated by the likely formation of charged transition states in solvents that are largely incapable of supporting them (e.g., C_6D_6). A further complication arises from the fact that HCl was added as a solution in Et_2O, thus the polarity of the solvent (C_6D_6:Et_2O mixture) is continuously changing. Regardless of the exact activation mechanism of **3.31** in C_6D_6 with HCl, the saturation behavior explains why a weaker acid (TFA) can, under some conditions, more efficiently activate **3.31** (e.g., Figure

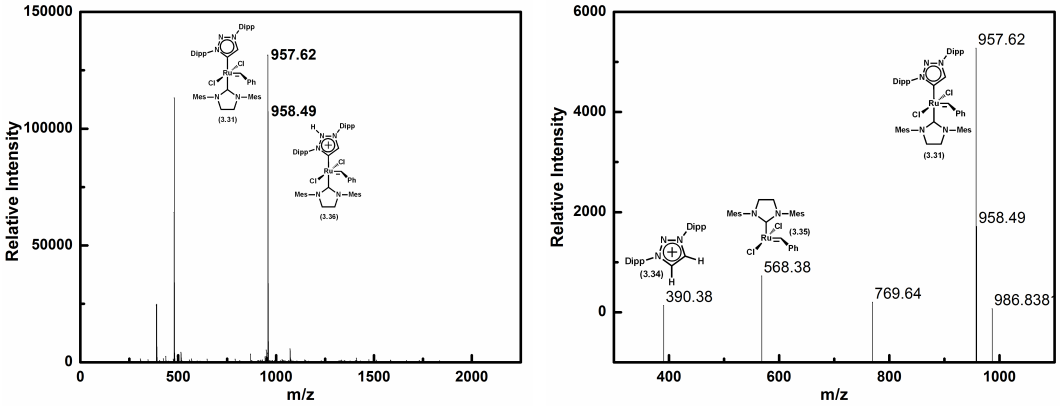

Figure 3.20. (left) Mass spec (ESI) of **3.31** immediately following addition of TFA. (right) Collision-induced dissociation (CID) of mass current 957.6 showing daughter peaks

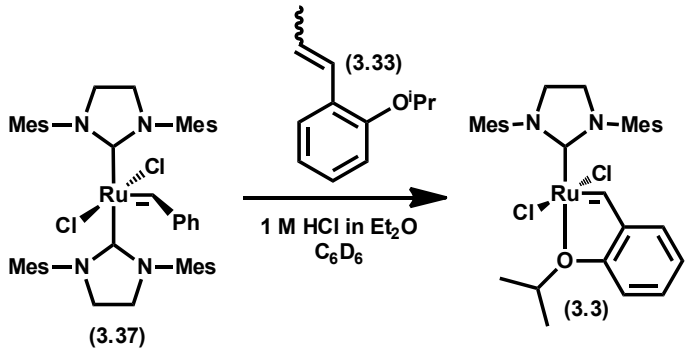

Figure 3.21. Initiation study of **3.37**. Conditions were **3.37** (0.0032 mmol), **3.33** (0.032 mmol), and HCl (0.05 mmol) in C_6D_6

3.12). Similarly, the observed initiation rate of **3.31** in C_6D_6 under saturation conditions at RT (0.0011 s^{-1}) is slightly higher than that of catalyst **3.2** (0.00046 s^{-1} at 35 °C),[3] which explains the superior performance of **3.31** in RCM compared to more conventional catalysts.

Continuing our mechanistic studies, the growth of product **3.3** was monitored after treatment of **3.31** with acid in the presence of varying amounts of olefin **3.33** as a trapping agent. A plot of k_{obs} for this reaction versus the concentration of **3.33** showed no dependence on **3.33** concentration, indicating that any reaction with olefin must take place after the rate-determining step has occurred (Figure 3.18).

The above experiment also allowed us to identify **3.34**, which precipitated from solution. Taken together, the formation of **3.3** and **3.34** suggests that protonation of **3.31** generates catalytic intermediate **3.35**, which is the same active species that is postulated to follow thermally induced ligand dissociation in common ruthenium metathesis catalysts.[3]

Unlike the initiation of traditional metathesis catalysts, which only slightly depends on solvent,[3] the various transformations depicted in Figure 3.19 are extremely sensitive to the identity of the solvent. For example, efficient initiation occurs in both C_6H_6 and CH_2Cl_2, as does metathesis activity. Similarly, efficient initiation also occurs (**3.31** to **3.35**) in CH_3CN; however, no catalytic activity is observed (**3.31** to **3.3**), presumably because **3.35** is immediately sequestered by solvent. In contrast to both of the above cases, the protonation event (**3.31** to **3.36**) does not occur (e.g., there is no disappearance of the benzylidene resonance) to any extent in THF. At this point, it is unclear why no reaction occurs in THF, but both the initiation mechanism and resulting catalytic activity are clearly highly dependent on the identity of the solvent.

A complete proposed initiation mechanism for **3.31** is shown in Figure 3.19. Although our mechanistic studies could not definitively establish the nature of the protonation event the fact that some Lewis acids also activated the catalyst strongly suggests that the unsubstituted nitrogen (N2) on the MIC ligand plans an important role. Previously reported density functional theory calculations on free MICs (e.g., **3.28**) indicate that N2 has the second-highest proton affinity after the carbene itself, meaning that protonation at this position is plausible.[13] Thus, it is likely that

initiation entails protonation at the MIC N2 in **3.31** to give **3.36**, followed by dissociation with a concomitant 1,3-proton shift to give **3.33** and **3.34**, both of which were observable by mass spectrometry (Figure 3.20). This mechanism is consistent with our experimental results to date, but at this time we cannot definitively rule out other possibilities, such as direct protonolysis of the Ru-MIC bond.

A final question we wished to answer was whether the behavior of **3.31** was due to the unique nature of the MIC ligand or if other conventional NHC (e.g., in **3.3**) would act in a similar manner. In order to determine this, $(H_2IMes)_2Cl_2Ru(=CHPh)$ (**3.37**) was added to **3.24**, and no RCM activity was observed at RT.[29] Upon addition of HCl (10 equiv.), no immediate activity was detected either. However, after a period of ca. 12 h at RT, ca. 70% conversion to **3.25** was observed by NMR spectroscopy. When HCl was added to a mixture of **3.37** and **3.33** in order to approximate the extent of catalyst initiation, only 12% conversion to catalyst **3.3** was achieved after a period of 24 h at RT (Figure 3.21). This result is in contrast to that observed for **3.31**, which was able to achieve complete conversion to **3.3** within a matter of minutes. Thus, although **3.37** is capable of being activated by acid, this occurs much less efficiently than for **3.31**. A similar conclusion was reached for complexes containing MICs **3.15**–**3.18**, which were efficiently activated with acid, but to a lesser extent than **3.31**.

Conclusions and Future Outlook

In summary, we have demonstrated that in the presence of acid, a MIC ligand may act as a leaving group, allowing an otherwise inactive metathesis complex (**3.31**) to enter the metathesis catalytic cycle. Furthermore, under

standard metathesis reactivity screening conditions, **3.31** was superior to the latest commercial catalysts and can complete RCM reactions with a matter of minutes at RT. A mechanistic study of the initiation mechanism concluded that protonation is the rate-determining step with the most efficient initiator, TFA, but that the activation step and resulting catalytic activity is strongly influenced by the identity of the acid and solvent. With strong-acid initiators, **3.31** was able to quickly and effectively access the same reactive intermediate as other catalysts (e.g., **3.3**) and thus combines latency with exceptional reactivity at RT. Finally, we established that the observed protonolysis behavior of **3.31** can also occur, but only to a limited extent in other bis-NHC complexes, enabling the incorporation of these activation mechanisms in future generations of metathesis catalysts.

Experimental

General Information: All reactions were carried out in dry glassware under an argon atmosphere using standard Schlenk line techniques or in a Vacuum Atmospheres Glovebox under a nitrogen atmosphere unless otherwise specified. Solvents were purified by passage through solvent purification columns and further degassed with argon.[30] NMR solvents were dried over CaH_2 and vacuum transferred to a dry Schlenk flask and subsequently degassed with argon. Commercially available reagents were used as received unless otherwise noted.

1D-NMR experiments were conducted on a Varian 600 MHz spectrometer equipped with a Triax (^{1}H, ^{13}C, ^{15}N) probe or a Varian Inova 400 Mhz spectrometer, while VT and kinetic experiments were conducted on a Varian 500 MHz spectrometer equipped with an AutoX probe. Accurate temperature measurements of the NMR

probe were obtained using a thermocouple connected to a multimeter with the probe immersed in an NMR tube containing a minimal amount of toluene. Experiments and pulse sequences from Varian's Chempack 4 software were used without modification except for changes in the number of FIDs and scans per FID. Reaction conversions were obtained by comparing the integral values of starting material and product, no internal standard was used. Chemical shifts are reported in ppm downfield from Me_4Si by using the residual solvent peak as an internal standard. Spectra were analyzed and processed using MestReNova Ver. 6.2.0 – 7163.[31]

High-resolution mass spectrometry (HRMS) data was obtained on a JEOL MSRoute mass spectrometer using FAB+ ionization. ESI-MS analyses were performed on a Finnigan LCQ classic mass spectrometer using the following conditions: spray voltage, 41 kV; sheath-gas flow rate, 20; cap. voltage, 5 V; cap. temp., 190 °C; tube lens voltage, 8 V; spectrum averaging, 10. In the daughter mode, a collision energy of 30 V was employed using He as the collision gas.

Ruthenium Complex 3.19: In a glovebox, a 20 mL scintillation vial was charged with carbene **3.15** (29 mg, 0.062 mmol),[13] catalyst **3.14** (29 mg, 0.048 mmol), and C_6H_6 (5 mL). The solution was stirred at RT for 10 h after which it was concentrated to a brown residue. The residue was dissolved in a minimal amount of CH_2Cl_2 and pentane was carefully layered on top. The vial was cooled to –30 °C for ca. 12 h at which point small brown crystals had crashed out. The solvent was decanted away and the crystals were washed with cold pentane (3X) and dried to give **3.19** (24 mg, 49%). ^{1}H NMR (400 MHz, C_6D_6) δ 16.83 (s, 1H), 8.47 (d, *J* = 7.5 Hz, 2H), 7.43 (t, *J* = 8 Hz, 1H), 7.30–7.17 (m, 6H), 7.16–7.01 (m, 4H), 7.01–6.92 (m, 1H),

6.82 (d, *J* = 7.8 Hz, 2H), 6.72 (td, *J* = 7.4, 0.7 Hz, 1H), 6.41 (d, *J* = 8.4 Hz, 1H), 4.53 (sept, *J* = 6.2 Hz, 1H), 3.11 (sept, *J* = 6.8 Hz, 2H), 2.81 (sept, *J* = 6.8 Hz, 2H), 1.56 (d, *J* = 6.1 Hz, 6H), 1.18 (d, *J* = 6.9 Hz, 6H), 1.15 (d, *J* = 6.7 Hz, 6H), 1.05 (d, *J* = 6.8 Hz, 6H), 0.93 (d, *J* = 6.8 Hz, 6H). ^{13}C NMR (101 MHz, C_6D_6) δ 165.31, 151.45, 145.96, 144.01, 142.92, 135.81, 134.23, 129.81, 129.70, 129.45, 127.50, 122.63, 122.43, 120.53, 119.35, 111.30, 72.93, 27.23, 27.03, 24.08, 23.84, 21.56, 20.57, 20.09. HRMS (FAB+): Calculated—785.2453, Found—785.2482.

Ruthenium Complex 3.20: 3.20 was prepared in a manner analogous to **3.19**. Carbene **3.16** (27 mg, 0.053 mmol), **3.14** (25 mg, 0.041 mmol), and PhH (2 mL). **3.20** (9 mg, 27%). ^{1}H NMR (400 MHz, CD_2Cl_2) δ 17.19 (s, 1H), 7.67 (t, *J* = 7.7 Hz, 1H), 7.55 (t, *J* = 7.8 Hz, 1H), 7.45 (m, 3H), 7.23 (d, *J* = 7.7 Hz, 2H), 7.09 (d, *J* = 7.5 Hz, 1H), 6.96 (s, 2H), 6.90 (m, 2H), 4.96 (sept, *J* = 6 Hz, 1H), 2.95 (sept, *J* = 6.8 Hz, 2H), 2.66 (sept, *J* = 6.8 Hz, 2H), 2.34 (s, 3H), 2.26 (s, 6H), 1.45 (d, *J* = 6.0 Hz, 6H), 1.33 (d, *J* = 6.5 Hz, 6H), 1.17 (d, *J* = 6.8 Hz, 6H), 1.13 (d, *J* = 6.5 Hz, 6H), 1.10 (d, *J* = 6.8 Hz, 6H). ^{13}C NMR (101 MHz, CD_2Cl_2) δ 287.37, 165.07, 152.74, 148.83, 148.39, 146.77, 145.53, 141.20, 140.48, 136.79, 131.85, 131.75, 130.35, 129.23, 128.80, 125.77, 125.17, 124.86, 124.35, 123.08, 121.74, 113.63, 75.41, 54.53, 54.26, 53.99, 53.72, 53.45, 30.11, 29.88, 29.63, 28.19, 27.53, 23.03, 22.67, 22.19, 22.10, 21.43. HRMS (FAB+): Calculated—827.2923, Found—827.2905.

Ruthenium Complex 3.21: 3.21 was prepared in a manner analogous to **3.19**. Carbene **3.17** (63 mg, 0.106 mmol), **3.14** (38 mg, 0.063 mmol), and PhH (3 mL). **3.21** (28.5 mg, 50%). ^{1}H NMR (500 MHz, CD_2Cl_2) δ 17.32 (s, 1H), 7.67 (t, *J* = 7.8

Hz, 1H), 7.54 (m, 2H), 7.49 (d, *J* = 7.8 Hz, 2H), 7.28 (d, *J* = 7.8 Hz, 2H), 7.24 (s, 2H), 6.99–6.82 (m, 2H), 5.10 (sept, *J* = 6 Hz, 1H), 3.17–2.96 (m, 4H), 2.80 (sept, *J* = 6.5 Hz, 2H), 2.49 (sept, *J* =6.5 Hz, 2H), 1.57 (d, *J* = 6.6 Hz, 6H), 1.53 (d, *J* = 6.2 Hz, 6H), 1.38 (d, *J* = 6.9 Hz, 6H), 1.20 (d, *J* = 6.8 Hz, 6H), 1.16 (d, *J* = 6.7 Hz, 6H), 0.87 (d, *J* = 6.6 Hz, 6H), 0.82–0.72 (m, 12H). ^{13}C NMR (126 MHz, CD_2Cl_2) δ 168.04, 152.68, 151.66, 150.40, 149.99, 148.20, 145.93, 135.35, 131.84, 131.09, 130.89, 128.26, 128.07, 125.03, 124.20, 123.78, 122.80, 122.43, 121.00, 113.09, 34.50, 30.97, 29.50, 29.29, 27.93, 27.31, 25.61, 23.83, 23.02, 22.89, 21.87, 21.62. HRMS (FAB+): Calculated—911.3862, Found—911.3891.

Ruthenium Complex 3.22: 3.22 was prepared in a manner analogous to **3.19**. Carbene **3.18** (69 mg, 0.181 mmol), **3.14** (84 mg, 0.139 mmol), and PhH (2 mL). **3.22** (12.4 mg, 12.7%). ^{1}H NMR (400 MHz, CD_2Cl_2) δ 16.89 (s, 1H), 8.13–8.05 (m, 2H), 7.66 – 7.52 (m, 2H), 7.49–7.42 (m, 2H), 7.22 (s, 2H), 7.17 (d, *J* = 7.1 Hz, 1H), 7.11 (dd, *J* = 7.6, 1.4 Hz, 1H), 7.04–6.93 (m, 3H), 5.09 (sept, *J* = 6.0 Hz, 1H), 2.55 (s, 3H), 2.34 (s, 3H), 2.18 (s, 6H), 2.11 (s, 6H), 1.62 (d, *J* = 6.1 Hz, 6H). ^{13}C NMR (101 MHz, CD_2Cl_2) δ 167.18, 163.85, 152.99, 145.21, 141.81, 141.59, 137.86, 137.27, 135.23, 135.01, 134.66, 132.82, 132.13, 130.95, 130.60, 130.54, 130.30, 129.98, 129.85, 129.74, 129.28, 129.12, 128.84, 128.69, 123.19, 121.95, 113.60, 75.42, 22.28, 21.69, 21.51, 18.17, 17.99. HRMS (FAB+): Calculated—701.1514, Found—701.1512

Representative Procedure for ROMP of 3.23: In a glovebox, a stock solution of **3.19** (3.6 mg, 0.0043 mmol) in C_6D_6 (1 mL) was prepared, and 93 μL ($4x10^{-4}$ mmol catalyst) of this solution was added to an NMR tube followed by 700 μL of C_6D_6.

The NMR tube was capped with a rubber septum, removed from the glovebox, and placed in the spectrometer where it was allowed to equilibrate at 30 °C. **3.23** (49 μL, 0.4 mmol) was injected through the septa (t = 0) and the tube was quickly inverted once and placed back into the spectrometer. Spectra were recorded by arraying the 'pad' function in vNMRj (starting time = 0 s, increment = 5 s). Percent conversion was determined by integration of the product peaks versus starting material peaks.

Representative Procedure for RCM of 3.24: 186 μL ($8x10^{-4}$ mmol) of the above stock solution was added to an NMR tube followed by 615 μL of C_6D_6. The NMR tube was capped with a rubber septum and placed in the spectrometer as before. **3.24** (19.3 μL, 0.08 mmol) was injected and spectra were recorded as described above.

Representative Procedure for RCM of 3.26: Kinetics for the RCM of **3.26** were performed in a manner analogous to **3.24**. **3.26** (20 μL, 0.08 mmol).

Initiation Rate Measurement and Eyring Plot. In a glovebox, a 2 mL volumetric flask was charged with **3.19** (19 mg, 0.024 mmol) and d_8-toluene (0.012 M). 0.25 mL (0.003 mmol catalyst) of the stock solution was added to an NMR tube followed by 0.35 mL of d_8-toluene. The tube was capped with a rubber septum, removed from the glovebox, and placed in the spectrometer where it was allowed to equilibrate at the desired temperature for ca. 10 min. The exact temperature was determined as described in the General Information. Butyl vinyl ether (12 μL, 0.09 mmol) was then injected through the septum and the NMR tube quickly

placed back into the spectrometer. The disappearance of the benzylidene proton resonance was monitored over time for at least three half-lives by arraying the 'pad' function in vNMRj. All reactions showed clean first-order kinetics and k_{obs} was determined from a plot of $\ln(C/C_0)$ versus time.

According to the Activated Complex Theory of Henry Eyring,

$$k=\left(\frac{k_B T}{h} e^{\Delta S^{\ddagger}/R}\right) e^{-\Delta H^{\ddagger}/RT} \qquad (1)$$

where k is the rate in s^{-1}, k_b is Boltzmann's constant, h is Planck's constant, R is the gas constant, and T is the temperature in Kelvin. Eq. 1 can be reworked to yield a linear equation which gives $\Delta H^{\ddagger}$ as the slope and $\Delta S^{\ddagger}$ as the intercept (Eq. 2).

$$R\ln\frac{hk}{k_b T} = \Delta S^{\ddagger} + \left(\frac{-1}{T}\right)\Delta H^{\ddagger} \qquad (2)$$

The uncertainty in the slope and intercept was determined directly from the output provided by the linear regression function of OriginPro 8.1.[32] The uncertainty in $\Delta G^{\ddagger}$ was calculated using the error in the slope, intercept, and the off-diagonal component of the variance-covariance matrix (because $\Delta H^{\ddagger}$ and $\Delta S^{\ddagger}$ are correlated) created by OriginPro.[33]

1,3-Bis(2,6-diisopropylphenyl)-1*H*-1,2,3-triazol-5-ylidene (3.28): Anhydrous THF (10 mL) is added to a stirred mixture of triazolium salt **3.28·HPF$_6$** (268 mg, 0.5 mmol) and potassium *tert*-butoxide (112 mg, 1.0 mmol) at 0 ˚C. The reaction mixture was stirred for 30 min at 0˚C, then warmed to room temperature while stirring for an additional 30 min. Volatiles were evaporated under reduced pressure, and dry benzene (20 mL) was added. The mixture was triturated for 15–30 min, and filtered

through a filter cannula. Evaporation of the solvents under reduced pressure afforded **3.28** (156 mg, 80%) as a pale yellow solid. M.p.: 141–143˚C (dec). *Note:* The NMR spectra of **3.28** presents some concentration-dependent broadening/ coalescence, attributed to the exchange of protons at the C4/C5 position. At low concentration in the presence of ~ 1 eq. residual PhMe, the spectra of **2** is clearly asymmetric, but shows some peak broadening, indicative of slow proton exchange at C4/C5 with respect to the NMR timescale. At higher concentrations, the exchange accelerates and the spectra of **3.28** becomes symmetric, and displays resonances at the expected midpoint chemical shifts of the low [**3.28**] resonances. *Low [3.28]:* ^{1}H NMR (C_6D_3, 300 MHz): δ = 7.53 (br s, 1H), 7.32 (br m, 1H), 7.20 (br m, 1H), 7.14–7.10 (m, 2H), 7.07–7.00 (m, 2H), 2.94 (br m, 2H), 2.47 (br m, 2H), 1.28 (br m, 6H), 1.23 (br m, 6H), 1.05 (br m, 12H). ^{13}C NMR (C_6D_6, 75 MHz): δ = 201.9 (C), 146.0 (C), 145.9 (C), 139.9 (C), 138.4 (CH), 133.9 (C), 131.4 (CH), 130.2 (CH), 124.4 (CH), 124.1 (CH), 29.2 (2 CH), 25.0 (CH_3), 24.8 (CH_3), 24.4 (CH_3), 24.2 (CH_3)

High [3.28]: ^{1}H NMR (C_6D_6, 300 MHz): δ = 7.56 (br s, 1H), 7.27 (t, *J* = 7.6 Hz, 2H), 7.10 (d, *J* = 7.7 Hz, 4H), 2.70 (br sept, *J* = 6.8 Hz, 4H), 2.47 (br m, 2H), 1.15 (d, *J* = 6.8 Hz, 12H), 1.11 (d, *J* = 6.8 Hz, 12H). ^{13}C NMR (C_6D_6, 75 MHz): δ = ~ 170 (br, C/CH), 145.9 (C), 136.8 (C), 130.8 (CH), 124.3 (CH), 29.2 (CH), 24.9 (CH), 24.2 (CH).

Ruthenium Complex 3.31: In a glovebox, a 20 mL scintillation vial was charged with MIC **3.28**[13] (208 mg, 0.535 mmol), **3.30**[34] (300 mg, 0.412 mmol), and C_6H_6 (7 mL). The brown solution was stirred for one hour and concentrated *in vacuo*

to a brown residue which was washed with cold pentane until the washes were colorless. The remaining brown solid was dried to give **3.31** (375 mg, 95%) which was subsequently lyophilized from C_6H_6. ^{1}H NMR (400 MHz, CD_2Cl_2) δ 18.52 (s, 1H), 7.53 (m, 3H), 7.33 (s, 1H), 7.31 (s, 1H), 7.20 (tt, J = 7.6, 0.8 Hz, 1H), 6.97–6.81 (m, 5H), 6.76 (d, J = 7.8 Hz, 2H), 6.59 (s, 1H), 6.28 (br s, 1H), 4.03–3.86 (m, 4H), 2.57 (s, 6H), 2.47 (sept, J = 6.8 Hz, 2H), 2.23 (sept, J = 6.8 Hz, 2H), 2.14 (br s, 6H), 2.00 (s, 3H), 1.93 (s, 3H), 1.17 (d, J = 6.8 Hz, 6H), 1.09 (d, J = 6.9 Hz, 6H), 1.05 (d, J = 6.6 Hz, 6H), 0.77 (d, J = 6.9 Hz, 6H). ^{13}C NMR (101 MHz, CD_2Cl_2) δ 225.91, 183.63, 150.56, 146.18, 145.84, 140.71, 137.07, 136.19, 134.23, 132.51, 131.98, 130.65, 130.44, 129.69, 129.31, 128.85, 127.53, 126.99, 125.39, 124.57, 123.32, 52.03, 51.79, 28.78, 28.60, 26.65, 25.38, 24.06, 22.22, 20.83, 18.62. HRMS (FAB+): Calculated—958.3896, Found—958.3917.

Representative Procedure for RCM of 3.24 with 3.31 and HCl: In a glovebox, a 1 mL volumetric flask was charged with **3.31** (5.6 mg, 0.0058 mmol) and filled to the 1 mL line with C_6D_6. A portion of the stock solution (140 µL, 0.0008 mmol **3.31**) was added to an NMR tube and diluted with C_6D_6 (660 µL). Compound **3.24** (19.3 µL, 0.08 mmol) was added and the NMR tube was capped with a rubber septum, removed from the glovebox, and placed inside the spectrometer. The tube was ejected and HCl (1M in Et_2O) (25 µL, 31 eq.) was injected after which the tube was quickly inverted once and placed back inside the spectrometer. An array of ^{1}H spectra were collected using the 'pad' function in vNMRj and processed according to the General Information.

Representative Procedure and Kinetic Plots for Reaction of 3.31 with HCl in

C_6D_6: In a glovebox, a 1 mL volumetric flask was charged with **3.31** (11.5 mg, 0.012 mmol) and filled to the 1 mL line with C_6D_6 to form a stock solution of catalyst. A portion (0.25 mL) of the stock solution above was transferred to an NMR tube and diluted with C_6D_6 (0.35 mL) such that the final concentration of **3.31** was ca. 0.005 M. The NMR tube was capped with a rubber septum, removed from the glovebox, and placed inside the spectrometer. After equilibration at the desired temperature for 10 min, HCl in Et_2O (between 5 and 50 μL) was injected through the rubber septum and the tube was quickly inverted once and placed back inside the spectrometer. An array of 1D ^1H spectra were collected using the 'pad' function in vNMRj.

Representative Procedure and Kinetic Plots for Reaction of 3.31 with HCl in C_6H_6 with Olefin 3.33: Inside a glovebox, an NMR tube with stock catalyst solution (0.25 mL) and C_6D_6 (0.35 mL) was prepared as above. Olefin **3.33** (1.6 uL, 0.009 mmol) was added along with anthracene (35 μL of a 0.086 M solution) as an internal standard and the tube was capped with a rubber septum and removed from the box. After equilibrating in the spectrometer, HCl (50 μL, 1 M in Et_2O) was added through the rubber septum and data was collected as above. Completion of the reaction was characterized by a change in color from yellow/brown to green and the formation of a white precipitate. The precipitate was collected by filtration and identified as **3.34** by ^1H NMR spectroscopy and HRMS (FAB+ : C – 390.2909, F – 390.2898). The green filtrate was concentrated and identified as **3.3** by HRMS (FAB+ : C – 626.1405, F – 626.1397) and ^1H NMR spectroscopy by comparison with authentic samples.

Eyring Plot Procedure (with Acid): In a glovebox, a 2 mL volumetric flask was charged with **3.31** (23 mg, 0.024 mmol) and filled to the line with d_8-toluene. A portion (0.25 mL) of the catalyst stock solution was added to an NMR tube and diluted with d_8-toluene (0.35 mL). The NMR tube was capped with a rubber septum, removed from the glovebox, and placed in the spectrometer at the desired temperature and allowed to equilibrate for ca. 10 min. The exact temperature of the NMR probe was determined as described in the General Information. After equilibrating, the tube was ejected and HCl (50 μL, 1 M in Et_2O) was added, after which the tube was inverted once and quickly placed back inside the spectrometer. Data was collected with the vNMRj array function as above. All reactions showed clean first-order kinetics over period of at least three half-lives and k_{obs} was determined from a plot of $\ln(C/C_0)$ versus time.

Mass Spectrometry Study of Reaction Mechanism: A 1 mM solution of **3.31** in C_6H_6 was prepared and TFA (5 μL) was added. The solution was loaded into a syringe and placed on a syringe pump connected to a mass spectrometer running on continuous electrospray ionization. Masses corresponding to SM and protonated SM were obtained (Figure 3.20). Parent and CID daughter peaks were collected according to the General Information.

Representative Procedure and Kinetic Plots for Reaction of 3.31 with TFA in C_6D_6: In a glovebox, a 1 mL volumetric flask was charged with **3.31** (13 mg, 0.0134 mmol) and filled to 1 mL with C_6D_6 to form a stock solution of catalyst. A portion of the stock solution (0.225 mL, 0.003 mmol **3.31**) was added to an NMR tube and diluted with C_6D_6 (0.375 mL). The NMR tube was capped with a rubber septum,

removed from the glovebox, and placed inside the spectrometer. TFA (0.026 mmol –0.091 mmol) was injected, the tube was inverted once, and placed back inside the spectrometer. Data was collected as above.

Representative Procedure and Kinetic Plots for Reaction of 3.31 with TFA in CD_3CN at Constant pH: In a glovebox, a 1 mL volumetric flask was charged with potassium trifluoroacetate (KTFA) (15 mg, 0.0986 mmol) which had been dried under vacuum at 70 °C for 12 h, and the flask was filled to the line with CD_3CN. A portion of the stock solution (30.4 µL, 0.003 mmol KTFA) was added to a vial containing **3.31** (2.9 mg, 0.003 mmol) and CD_3CN (0.570 mL). The resulting fine suspension was shaken and quickly transferred to an NMR tube which was capped with a rubber septum. (Note : Over prolonged periods of time (hours), **3.31** would decompose in the presence of CD_3CN, therefore, all samples for kinetic runs were prepared immediately prior to use.) The NMR tube was removed from the glovebox and placed inside the spectrometer. TFA (3.4 µL, 0.045 mmol) was injected through the rubber septum and the tube was quickly inverted before being placed back inside the spectrometer. NMR spectra were recorded as described previously.

Representative Procedure for Brønsted Plot: In a glovebox, a 1 mL volumetric flask was charged with **3.31** (9.7 mg, 0.01 mmol) and filled to the line with CD_3CN to make a 0.01 M stock solution. An aliquot of the stock solution (300 µL) was added to an NMR tube and diluted with CD_3CN (300 µL). The NMR tube was capped with a rubber septum, removed from the glovebox, and placed inside the spectrometer. TFA (3.5 µL, 0.045 mmol, 15 eq.) was injected after which the

tube was inverted once and placed back inside the spectrometer. Spectra were recorded periodically as described above. The same procedure was repeated for the following acids: Methane-sulfonic acid (3 μL, 0.045 mmol), Dichloroacetic acid (3.7 μL, 0.045 mmol), and Acetic acid (2.6 μL, 0.045 mmol). Acid dissociation constants in acetonitrile were estimated from Eq. 3[35] using pK_a values in DMSO.[36]

$$pK_a(AN) = b + apK_a(DMSO) \qquad (3)$$

$$b = 11.80 \; a = 0.884$$

Representative Procedure and Kinetic Plots for Reaction of 3.31 with TFA in CD_3CN Containing Varying Amounts of KTFA (Variable pH): A 1 mL volumetric flask was charged with KTFA (13.6 mg, 0.0907 mmol) and filled to the line with CD_3CN. A portion of the KTFA stock solution (55 μL, 0.005 mmol) was transferred to a vial containing **3.31** (2.9 mg, 0.003 mmol) and CD_3CN (550 μL). The resulting suspension was quickly shaken and transferred to an NMR tube and capped with a rubber septa. TFA (3.4 μL, 0.045 mmol) was injected and the tube was quickly inverted and placed inside the spectrometer. Spectra were recorded as above.

Representative Procedure and Kinetic Plots for Reaction of 3.31 with HCl (1 M in Et_2O) in CD_3CN: In a glovebox, a 4 mL vial was charged with **3.31** (2.9 mg, 0.003 mmol) and CD_3CN (0.6 mL). The fine suspension was transferred to an NMR tube which was capped with a rubber septum and removed from the box. The NMR tube was placed inside the spectrometer and equilibrated at 25 °C after which it was ejected and HCl (1 M in Et_2O, 5 μL) was added via syringe. After inverting once, the tube was placed back inside the spectrometer and data was

collected as above. Note that in the case of a small amount of HCl (5 μL), pseudo-first-order conditions are not applicable. Therefore, only the first few minutes of the reaction were used to obtain k_{obs}. All other amounts of HCl displayed good first-order behavior until completion of the reaction.

References

(1) (a) Fürstner, A. *Angew. Chem. Int. Ed.* **2000**, *39*, 3012. (b) Trnka, T. M.; Grubbs, R. H. *Acc. Chem. Res.* **2001**, *34*, 18. (c) Astruc, D. *New J. Chem.* **2005**, *29*, 42.

(2) (a) Kinsgbury, J. S.; Harrity, J. P.; Bonitatebus, P. J.; Hoveyda, A. H. *J. Am. Chem. Soc.* **1999**, *121*, 791. (b) Garber, S. B.; Kingsbury, J. S.; Gray, B. L.; Hoveyda, A. H. *J. Am. Chem. Soc.* **2000**, *122*, 8168. (c) Hong, S. H.; Day, M. W.; Grubbs, R. H. *J. Am. Chem. Soc*. **2004**, *126*, 7414. (d) Hong, S. H.; Wenzel, A. G.; Salguero, T. T.; Day, M. W.; Grubbs, R. H. *J. Am. Chem. Soc*. **2007**, *129*, 7961. (e) Hong, S. H.; Chlenov, A.; Day, M. W.; Grubbs, R. H. *Angew. Chem. Int. Ed*. **2007**, *46*, 5148. (f) Vehlow, K.; Gessler, S.; Blechert, S. *Angew. Chem. Int. Ed*. **2007**, *46*, 8082. (g) Leitao, E. M.; Dubberley, S. R.; Piers, W. E.; Wu, Q.; McDonald, R. *Chem. Eur. J*. **2008**, *14*, 11565. (h) Mathew, J.; Koga, N.; Suresh, C. H. *Organometallics* **2008**, *27*, 4666.

(3) Sanford, M. S.; Love, J. A.; Grubbs, R. H. *J. Am. Chem. Soc.* **2001**, *123*, 6543.

(4) Getty, K.; Delgado-Jaime, M. U.; Kennepohl, P. *J. Am. Chem. Soc.* **2007**, *129*, 15774.

(5) (a) Samojłowicz, C.; Bieniek, M.; Grela, K. *Chem. Rev.* **2009**, *109*, 3708. (b) Vougioukalakis, G. C.; Grubbs, R. H. *Chem. Rev.* **2010**, *110*, 1746.

(6) Bourgeois, D.; Pancrazi, A.; Nolan, S. P.; Prunet, J. *J. Organomet. Chem.* **2002**,

643–644, 247.

(7) (a) Arnold, P. L.; Pearson, S. *Coord. Chem. Rev.* **2007**, *251*, 596 (b) Albrecht, M. *Chem. Commun.* **2008**, 3601 (c) Schuster, O.; Yang, L.; Raubenheimer, H. G.; Albrecht, M. *Chem. Rev.* **2009**, *109*, 3445 (d) Albrecht, M. *Chimia* **2009**, *63*, 105. For comparisons of the properties of normal, abnormal, and remote carbenes, see for examples: (e) Heydenrych, G.; von Hopffgarten, M.; Stander, E.; Schuster, O.; Raubenheimer, H. G.; Frenking, G. *Eur. J. Inorg. Chem.* **2009**, 1892 (f) Stander-Grobler, E.; Schuster, O.; Heydenrych, G.; Cronje, S.; Tosh, E.; Albrecht, M.; Frenking, G.; Raubenheimer, H. G. *Organometallics* **2010**, *29*, 5821.

(8) (a) Lavallo, V.; Canac, Y.; Präsang, C.; Donnadieu, B.; Bertrand, G. *Angew. Chem. Int. Ed.* **2005**, *117*, 5851. (b) Lavallo, V.; Canac, Y.; DeHope, A.; Donnadieu, B.; Bertrand, G. *Angew. Chem. Int. Ed.* **2005**, *117*, 7402. (c) Anderson, D. R.; Lavallo, V.; O'Leary, D. J.; Bertrand, G.; Grubbs, R. H. *Angew. Chem. Int. Ed.* **2007**, *46*, 7262. (d) Anderson, D. R.; Ung, T. A.; Mkrtumyan, G.; Bertrand, G.; Grubbs, R. H.; Schrodi, Y. *Organometallics* **2008**, *27*, 563.

(9) IUPAC. Compendium of Chemical Terminology, 2nd ed. (the "Gold Book"). Compiled by A. D. McNaught and A. Wilkinson. Blackwell Scientific Publications, Oxford (1997). XML on-line corrected version: http://goldbook.iupac.org (2006) created by M. Nic, J. Jirat, B. Kosata; updates compiled by A. Jenkins. ISBN 0-9678550-9-8. doi:10.1351/goldbook

(10) a) Grundemann, S.; Kovacevic, A.; Albrecht, M.; Faller, J. W.; Crabtree, R. H. *Chem. Commun.* **2001**, 2274 (b) Grundemann, S.; Kovacevic, A.; Albrecht, M.; Faller, J. W.; Crabtree, R. H. *J. Am. Chem. Soc.* **2002**, *124*, 10473.

(11) Guisado-Barrios, G.; Bouffard, J.; Donnadieu, B.; Bertrand, G. *Angew. Chem. Int. Ed.* **2010**, *49*, 4759.

(12) Alder, R. W.; Blake, M. E.; Chaker, L.; Harvey, J. N.; Paolini, F.; Schütz, J. *Angew. Chem. Int. Ed.* **2004**, *43*, 5896.

(13) Bouffard, J.; Keitz, B. K.; Tonner, R.; Guisado-Barrios, G.; Frenking, G.; Grubbs, R. H.; Bertrand, G. *Organometallics* **2011**, *30*, 2617.

(14) Gessler, S.; Randl, S.; Blechert, S. *Tetrahedron Lett.* **2000**, *41*, 9973.

(15) Van Veldhuizen, J. J.; Garber, S. B.; Kingsbury, J. S.; Hoveyda, A. H. *J. Am. Chem. Soc.* **2002**, *124*, 4954.

(16) Ragone, F.; Poater, A.; Cavallo, L. *J. Am. Chem. Soc.* **2010**, *132*, 4249.

(17) Ritter, T.; Hejl, A.; Wenzel, A. G.; Funk, T. W.; Grubbs, R. H. *Organometallics* **2006**, *25*, 5740.

(18) Hejl, A. S. Thesis, California Institute of Technology, 2007.

(19) (a) Vorfalt, T.; Wannowius, K.-J.; Plenio, H. *Angew. Chem. Int. Ed.* **2010**, *49*, 5533. (b) Ashworth, I. W.; Hillier, I. H.; Nelson, D. J.; Percy, J. M.; Vincent, M. A.*Chem. Commun.* **2011**, *47*, 5428. (c) Thiel, V.; Hendann, M.; Wannowius, K.-J.; Plenio, H. *J. Am. Chem. Soc.* **2012**, *134*, 1104.

(20) (a) da Costa, R. C.; Hampel, F.; Gladysz, J. *Polyhedron* **2007**, *26*, 581. (b) Leitao, E. M.; van der Eide, E. F.; Romero, P. E.; Piers, W. E.; McDonald, R. *J. Am. Chem. Soc*. **2010**, *132*, 2784.

(21) (a) Simonovic, S.; Whitwood, A. C.; Clegg, W.; Harrington, R. W.; Hursthouse, M. B.; Male, L.; Douthwaite, R. E. *Eur. J. Inorg. Chem*. **2009**, *2009*, 1786. (b) McGuinness, D. S.; Yates, B. F.; Cavell, K. J. *Chem. Commun*. **2001**, 355. (c)

Wang, C.-Y.; Liu, Y.-H.; Peng, S.-M.; Chen, J.-T.; Liu, S.-T. *J. Organomet. Chem*. **2007**, *692*, 3976. (d) Blue, E.; Gunnoe, T.; Petersen, J.; Boyle, P. *J. Organomet. Chem*. **2006**, *691*, 5988. (e) Fu, C.-F.; Lee, C.-C.; Liu, Y.-H.; Peng, S.-M.; Warsink, S.; Elsevier, C. J.; Chen, J.-T.; Liu, S.-T. *Inorg. Chem.* **2010**, *49*, 3011. (f) Díez-González, S.; Nolan, S. P. *Angew. Chem. Int. Ed.* **2008**, 47, 8881.

(22) When no acid was added, **3.31** began to show evidence of polymerization at temperatures of ca. 60 °C, indicating that thermal initiation is also viable.

(23) Ritter, T.; Hejl, A.; Wenzel, A. G.; Funk, T. W.; Grubbs, R. H. *Organometallics* **2006**, *25*, 5740.

(24) Bielawski, C. W.; Grubbs, R. H. *Prog. Poly. Sci.* **2007**, *32*, 1.

(25) (a) Fujii, Y; Kawachi, Y.; Tanaka, M. *J. Chem. Soc., Faraday Trans.* **1981**, 63. (b) Zaugg, N. S.; Kelley, A. J.; Woolley, E. M. *J. Chem. Eng. Data*. **1979**, *24*, 218. (c) Nagai, Y.; Simamura, O. *Bull. Chem. Soc. Japan* **1962**, *2*, 132.

(26) Jencks, W. *Acc. Chem. Res*. **1980**, *13*, 161.

(27) Lewis, E. W. *J. Phys. Org. Chem.* **1990**, *3*, 1.

(28) For likely structures of HCl in PhH see : Buch, V.; Mohamed, F.; Krack, M.; Sadlej, J.; Devlin, J. P.; Parrinello, M. *J. Chem. Phys*. **2004**, *121*, 12135.

(29) Trnka, T. M.; Morgan, J. P.; Sanford, M. S.; Wilhelm, T. E.; Scholl, M.; Choi, T.-L.; Ding, S.; Day, M. W.; Grubbs, R. H. *J. Am. Chem. Soc.* **2003**, *125*, 2546.

(30) Love, J. A.; Morgan, J. P.; Trnka, T. M.; Grubbs, R. H. *Angew. Chem. Int. Ed.* **2002**, *41*, 4035.

(31) www.mestrelab.com

(32) http://www.originlab.com/index.aspx?go=Products/OriginPro

(33) For a more detailed explanation on the method used to calculate the uncertainty in $\Delta G^{\ddagger}$ see: Anderson, D. R.; Hickstein, D. D.; O'Leary, D. J.; Grubbs, R. H. *J. Am Chem. Soc*. **2006**, *128*, 8386.

(34) Love, J. A.; Sanford, M. S.; Day, M. W.; Grubbs, R. H. *J. Am. Chem. Soc.* **2003**, *125*, 10103.

(35) Kütt, A.; Leito, I.; Kaljurand, I.; Sooväli, L.; Vlasov, V. M.; Yagupolskii, L. M.; Koppel, I. A. *J. Org. Chem*. **2006**, *71*, 2829.

(36) Ding, F.; Smith, J. M.; Wang, H. *J. Org. Chem.* **2009**, *74*, 2679 and references therein.